

Coherent rotation of magnetization in three dimensions: A geometrical approach

André Thiaville

CNRS–Université Paris-Sud, Laboratoire de Physique des Solides, 91405 Orsay, France

(Received 20 September 1999)

We propose a geometrical method to explore the problem of coherent magnetization rotation, for an arbitrary anisotropy and in three dimensions. This method is a nontrivial generalization of the astroid construction which is well known in two dimensions. Specific features to the three-dimensional (3D) problem are highlighted. In order to establish a connection with the thermal and quantum theories of magnetization relaxation, the local curvatures of the potential are also evaluated geometrically. As an application of the method to a real 3D problem, the determination of the effective anisotropy constants from 3D switching field measurements is discussed and first results shown.

I. INTRODUCTION

Coherent rotation (hereafter CR) of magnetization is one of the basic processes by which a ferromagnetic body responds to a field. The other competing processes are domain-wall propagation and domain nucleation. Depending on the sample size and shape, its intrinsic magnetic properties, and the time dependence of the applied field, one of the processes may dominate. Schematically, CR is to be expected at very small sample sizes (the single domain limit, where domain walls cannot fit in the sample) and at high fields in samples with low coercivity. In the CR regime, the sample magnetization is uniform, its static orientation (unit vector \vec{m}) being the solution of

$$\min_{|\vec{m}|=1} [KV_{\vec{H}}(\vec{m}) \equiv KG(\vec{m}) - M_s \vec{m} \cdot \vec{H}], \quad (1)$$

where K is an effective anisotropy constant, G the function describing the angular dependence of the anisotropy, M_s the saturation magnetization density, and \vec{H} the applied field. Comparing Eq. (1) with the usual micromagnetic energy functional, one sees that the exchange and demagnetizing energy terms have disappeared. Exchange energy is zero because of the assumption of a uniform \vec{m} . The demagnetizing term has the same form as that of an ellipsoid when the sample is uniformly magnetized,¹ and can therefore be included into the effective anisotropy as a second degree polynomial. More generally, the effective anisotropy is the sum of contributions from crystalline bulk anisotropy (any degree), surface anisotropy and magnetostatic energy.

Despite its simplicity, the problem (1) conceals a wide variety of magnetic behaviors and does not allow for an analytic solution in the general case. The first systematic study of CR was performed by Stoner and Wohlfarth,² in the simplest case where G is uniaxial and of second degree. They derived the ubiquitous easy axis and hard axis hysteresis loops, and tabulated those for any angle between field and easy axis. In the Stoner-Wohlfarth problem, the plane defined by the easy axis and the field contains also the (static) magnetization, so that it reduces to a two-dimensional (2D) problem. That paper therefore had a great impact on the soft magnetic thin-films research that developed later, as the magnetization in soft thin films is confined to the film plane by a demagnetizing field much larger than the anisotropy

field (see Ref. 3 for a review). The problem that comes next to attention, namely that of a cubic anisotropy (fourth degree at least), is 3D and not amenable to the same solution level as the preceding one. The parameter space is now two dimensional (the polar and azimuthal angles of \vec{m}), and the number of metastable states near zero field increases to 6 or 8, depending on the sign of K . Moreover, as shown numerically by Johnson,⁴ in case of a magnetization jump the final state is manyfold. The guess that it should be the lowest energy state is already disproved in 2D.⁵ In order to find the final state, the dynamic equation has to be solved, and it is easy to conceive that parameters such as the field sweep rate will greatly affect the outcome of the calculation. Thus *static* hysteresis loops in 3D are ill defined in principle, and the 3D problem is richer than the 2D one.

An alternative approach to numerics, namely geometry, was proposed by J. Slonczewski⁶ and became known as the astroid method. In essence, it considers instead of the magnetization direction \vec{m} the field \vec{H} as the main variable. As the potential $KG(\vec{m}) - M_s \vec{H} \cdot \vec{m}$ is linear in field, the extremum condition in \vec{m} is satisfied, for a fixed \vec{m} , along straight lines in the field space. Slonczewski worked out the 2D uniaxial second degree case, but the method treats any 2D problem alike (see Ref. 7 for one example, and Ref. 5 for a general formulation of the 2D case). The geometrical method introduces a curve in the field plane, called the critical curve (a square astroid in the original paper) to which the straight lines are tangent, these lines being parallel to \vec{m} . The critical curve is additionally the locus of fields at which a magnetization jump occurs. The stable solutions lie on one half of the straight lines, that starts at the critical curve and extends in the direction of \vec{m} . The traditional use of the astroid is to visualize the switching fields and to construct \vec{m} from \vec{H} graphically. In a previous paper⁵ an extensive study of the general case in 2D was performed, in which it was moreover shown that the energy of the system could be calculated geometrically. It is one purpose of this paper to treat the general case of an arbitrary $G(\vec{m})$ in three dimensions, trying to parallel the work in 2D as much as possible. It will be shown that the critical curve is replaced by one critical surface, the locus of fields at which a jump of magnetization occurs, plus a second surface. The straight lines directed along \vec{m} are

tangent to both surfaces, and on each surface they are tangent to a set of special curves covering the surface which we introduce. Energy can again be calculated with these curves.

The motivation for this work is multiple. The main field of application of the CR model is magnetic nanoparticles. For a long period of time, only macroscopic measurements were possible on such samples, so that the exact behavior of each particle was diluted by averaging over the distributions of particle shape, size and orientation. Nevertheless, these macroscopic measurements showed that even nanoparticles were sometimes more complex than single domain.^{8,9} At nanometer sizes, the atoms at surface are in comparable number to those in the interior, so that surface magnetism effects become as important as bulk ones. It was found that the type of particle magnetic order (ferromagnetic, ferrimagnetic,⁸ antiferromagnetic¹⁰) and the chemical state of the surface (e.g., carbon passivated, oxidized) are key parameters controlling the magnetic properties of the nanoparticles. As a result, a global understanding of the magnetic properties of nanoparticles has not yet been reached. One can hope that measurements on isolated particles will help to clear up the situation. In order to be able to interpret such data, the very peculiarities of each measured particle have to be taken in account, among which its effective anisotropy. We believe that a geometrical method can be of great value in developing some feeling about the behavior of a given particle in various situations, in the case of CR which is the simplest approximation. As an example, experimental 3D switching fields surfaces measured on isolated nanoparticles will be fitted by surfaces generated using the geometrical procedure, in order to find out their effective anisotropy. Even in cases where CR is thought not to be an adequate model, it is necessary to know what the detailed predictions of CR are in order to disprove them.

In cases where CR applies, the particle magnetization relaxation in temperature and at zero temperature is yet a largely open field (see Ref. 11 for a review of the various models), to which the geometrical method can contribute. In the thermal regime, the early models of Néel and Brown predict an exponential relaxation, in the case of uniaxial anisotropy. The relaxation time is written as

$$\tau = \tau_0 \exp(E_B/kT), \quad (2)$$

where E_B denotes the barrier in energy that has to be overcome in order to exit from the metastable state. The prefactor τ_0 is still the subject of much debate. Néel derived an expression from the magnetoelastic interactions. Brown introduced the Fokker-Planck approach in the problem (i.e., considered a continuous distribution of orientations) and derived from the Landau-Lifshitz-Gilbert (LLG) equation the evolution of this distribution. The prefactor found with some approximations is typically expressed as

$$\tau_0 = 4\pi \frac{1 + \alpha^2}{\alpha} \frac{1}{\gamma H_K} f(H), \quad (3)$$

where α is the Gilbert damping parameter, γ the gyromagnetic ratio, H_K the anisotropy field, and $f(H)$ a geometrical factor that diverges algebraically at the jump field. The generalization of Eq. (3) to less symmetric cases has been the subject of much recent work. The most general expressions are^{12,13}

$$\tau_0 = 4\pi \frac{1 + \alpha^2}{\alpha} \frac{1}{\gamma H_K} \times \frac{2\sqrt{-c_1 c_2}}{-c_1 - c_2 + \sqrt{(c_1 - c_2)^2 - 4c_1 c_2 / \alpha^2}} \frac{1}{\sqrt{c_1^{(1)} c_2^{(1)}}} \quad (4)$$

in the so-called intermediate to high damping case, and

$$\tau_0 = \frac{4\pi}{\alpha} \frac{1}{\gamma H_K} \frac{1}{\sqrt{c_1^{(1)} c_2^{(1)}}} \frac{kT}{E_B} \quad (5)$$

in the low damping case. In these expressions, c_1 and c_2 are the two eigenvalues of the second-order form of $V_{\vec{H}}(\vec{m})$ at barrier top (saddle point, thus $c_1 > 0, c_2 < 0$), and $c_1^{(1)}$ and $c_2^{(1)}$ those values at the metastable position (both positive). The geometrical factor $f(H)$ in Eq. (3) is thus related to the curvature of the potential $V_{\vec{H}}(\vec{m})$. In the quantum regime, an exponential relaxation by tunneling is also expected, with a characteristic time given by (see Ref. 14, for example)

$$\tau^{-1} = C_0 \sqrt{\frac{S}{2\pi\hbar}} \omega_t \exp\left(-\frac{S}{\hbar}\right). \quad (6)$$

In this expression, S is the action evaluated with the so-called instanton solution of the classical equations of motion (here LLG, without damping), ω_t the precession frequency of that solution and C_0 a numerical factor. As a rule of thumb, the action S is of the order of E_B/ω_b (E_B is the barrier height considered before, ω_b the oscillation frequency in the metastable potential well), and $\omega_t \approx \omega_b$. Explicit formulas were derived in a large number of cases,^{15,14} including hexagonal and cubic symmetry with the field within special planes. But no general expression like Eqs. (4) or (5) existed up to now. Using the general estimates mentioned above shows however that the evaluations of the barrier height and the curvature of $V_{\vec{H}}(\vec{m})$ are again required in order to predict the tunneling rate. The same quantities also enter the expression of the oscillation rate in the macroscopic quantum coherence regime.¹⁴ Therefore we see that the essential quantities governing the magnetization dynamics are the potential's curvatures and the energy barrier. Note also that the ferromagnetic resonance frequency is directly calculated from the curvature of the potential. It will be shown here how the geometrical approach allows for their determination, and the geometrical significance they have.

The paper is organized as follows. Section II gives the main results of the geometrical solution for an arbitrary $G(\vec{m})$. The underlying mathematics is exposed more in depth in the Appendix. Problems having a revolution symmetry are examined in Sec. III. The differences with the 2D solution, due to the additional degree of freedom, are discussed. Section IV studies in detail the biaxial case $G = m_x^2 + Am_y^2$, which constitutes the first nontrivial extension of the 2D square astroid. Examples of application of the method to experimental data obtained on isolated nanoparticles (measurements by E. Bonet-Orozco and W. Wernsdorfer at L.L.N. Grenoble) are shown in Sec. V. Anisotropy functions are extracted from switching field measurements. The difficulties of the procedure are discussed.

II. GEOMETRICAL SOLUTION

A. The two critical surfaces

The starting point is the potential

$$V_{\vec{H}}(\vec{m}) = G(\vec{m}) - 2\vec{h} \cdot \vec{m}, \quad (7)$$

where \vec{h} is the normalized field \vec{H}/H_K (the anisotropy field H_K is defined as $2K/M_s$). The unit vector \vec{m} is described by the polar angle θ relative to some axis Oz , and the azimuthal angle ϕ . An orthonormal direct basis is formed by the three vectors \vec{m} , $\vec{e}_\theta = \partial\vec{m}/\partial\theta$ and $\vec{e}_\phi = (1/\sin\theta)\partial\vec{m}/\partial\phi$. $V_{\vec{H}}$ has to be stationary in \vec{m} , thus

$$\begin{aligned} G_\theta - 2\vec{h} \cdot \vec{e}_\theta &= 0, \\ G_\phi - 2\sin\theta\vec{h} \cdot \vec{e}_\phi &= 0 \end{aligned} \quad (8)$$

(G_θ stands for $\partial G/\partial\theta$, etc.). In the field plane, Eq.(8) is that of a straight line, which can be described with a parameter λ as

$$\vec{h} = \frac{1}{2}G_\theta\vec{e}_\theta + \frac{1}{2\sin\theta}G_\phi\vec{e}_\phi + \lambda\vec{m}. \quad (9)$$

Stable solutions have $V_{\vec{H}}$ locally minimum at \vec{m} . The second derivatives of the potential read

$$\begin{aligned} V_{\theta\theta} &= G_{\theta\theta} + 2\vec{h} \cdot \vec{m} = G_{\theta\theta} + 2\lambda, \\ V_{\theta\phi} &= G_{\theta\phi} - 2\cos\theta\vec{h} \cdot \vec{e}_\phi = \sin\theta \frac{\partial}{\partial\theta} \left(\frac{G_\phi}{\sin\theta} \right), \\ V_{\phi\phi} &= G_{\phi\phi} + 2\sin\theta\vec{h} \cdot (\sin\theta\vec{m} + \cos\theta\vec{e}_\theta) \\ &= G_{\phi\phi} + \sin\theta\cos\theta G_\theta + 2\lambda\sin^2\theta. \end{aligned} \quad (10)$$

The stability requires that both eigenvalues of this matrix are positive, thus that their sum $V_{\theta\theta} + V_{\phi\phi}$ and their product $V_{\theta\theta}V_{\phi\phi} - (V_{\theta\phi})^2$ are positive. The sum is linear in λ with a positive coefficient, the product is quadratic with positive λ^2 coefficient. The two zeros of the product are real and expressed as

$$\begin{aligned} \lambda_\pm &= \frac{1}{4} \left[- \left(\frac{G_{\phi\phi}}{\sin^2\theta} + \frac{\cos\theta}{\sin\theta} G_\theta + G_{\theta\theta} \right) \right. \\ &\quad \left. \pm \sqrt{\left(\frac{G_{\phi\phi}}{\sin^2\theta} + \frac{\cos\theta}{\sin\theta} G_\theta - G_{\theta\theta} \right)^2 + 4 \left[\frac{\partial}{\partial\theta} \left(\frac{G_\phi}{\sin\theta} \right) \right]^2} \right]. \end{aligned} \quad (11)$$

Therefore the half line (9) described by $\lambda \geq \lambda_+$ is the locus of the fields for which the magnetization \vec{m} is stable. At $\lambda = \lambda_+$ one eigenvalue falls to 0, and the magnetization vector can escape from the potential well. Between λ_+ and λ_- one eigenvalue is positive and one negative: the potential is locally of saddle shape. Saddle points also deserve consideration because, as described in the introduction, they influence the magnetization dynamics. Below λ_- both eigenvalues are negative and the potential is at a maximum. Setting $\lambda = \lambda_+$ or $\lambda = \lambda_-$ in Eq. (9) generates two surfaces, parametrized by θ and ϕ , which we denote by S_+ and S_- . S_+ is the locus of the fields at which the magnetization un-

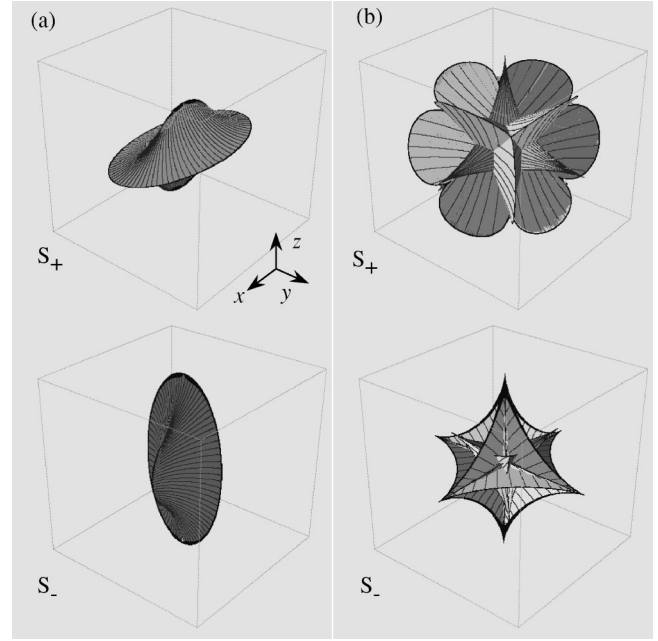


FIG. 1. Perspective view of the two critical surfaces S_+ and S_- in the two simple cases of a biaxial symmetry $G = m_x^2 + 0.5m_y^2$ (a) and a cubic symmetry $G = m_x^2m_y^2 + m_y^2m_z^2 + m_z^2m_x^2$ (b). The cubic box has sides of length 2. Various parts (called ‘‘bells’’ hereafter) of the S_+ surfaces have been stained differently. The focal curves that cover the surfaces and cusp lines (where the surface is folded) are also drawn. With the biaxial symmetry (a), both surfaces are built out of two halves glued along the ellipse. The focal curves on S_+ start from the ‘‘handle cusps’’ and end on the elliptical cusp. In the cubic case (b), S_+ consists in 6 gramophonelike bells, each bell being four leaved and starting from one point (there are also tiny surface parts close to the $\{111\}$ directions). The bells have a $\{100\}$ orientation and correspond to the easy directions of a positive cubic anisotropy. Conversely, S_- consists in eight tripods with the $\{111\}$ orientations, like the easy directions for a negative cubic anisotropy. This last surface was colored so as to display its various pieces.

dergoes a jump towards another stable orientation. This surface, as it generalizes the critical curve of the 2D problem, is called the critical surface. S_- is another surface, unnecessary at first sight (of course, upon changing G to $-G$, S_+ and S_- would exchange roles). The interest of S_- will become apparent later. Figure 1 displays these surfaces in several high symmetry cases. The higher the degree of G the more complex they become. The surface S_+ of the cubic case [Fig. 1(b)] bears some resemblance with the drawing of the two-phase boundaries and critical curves for the same anisotropy.¹⁶ The zooms near the $[111]$ axis also have the same topology (not shown here). This should be no surprise, as phase theory in magnetism also considers uniform magnetizations. The two-phase boundaries (fields where two solutions have the same energy) are the symmetry planes of the ‘‘leaves’’ of S_+ , with $\{110\}$ orientations. The curves that end the two-phase regions mark the onset of the one solution regime, and are identical to the end cusps that will be introduced below. Note that phase theory drawings do not provide a construction of the magnetization.

The tangential planes to the surfaces S_\pm are now considered. The partial derivatives of \vec{h} are

$$\begin{aligned}\frac{\partial \vec{h}}{\partial \theta} &= \frac{1}{2}(G_{\theta\theta} + 2\lambda)\vec{e}_\theta + \frac{1}{2}\frac{\partial}{\partial \theta}\left(\frac{G_\phi}{\sin\theta}\right)\vec{e}_\phi + \left(\frac{\partial \lambda}{\partial \theta} - \frac{1}{2}G_\theta\right)\vec{m}, \\ \frac{\partial \vec{h}}{\partial \phi} &= \frac{1}{2}\sin\theta\frac{\partial}{\partial \theta}\left(\frac{G_\phi}{\sin\theta}\right)\vec{e}_\theta + \frac{1}{2\sin\theta}(G_{\phi\phi} + \sin\theta\cos\theta G_\theta \\ &\quad + 2\lambda\sin^2\theta)\vec{e}_\phi + \left(\frac{\partial \lambda}{\partial \phi} - \frac{1}{2}G_\phi\right)\vec{m}.\end{aligned}\quad (12)$$

The normal to the surface is directed along the vector product $\partial\vec{h}/\partial\theta \wedge \partial\vec{h}/\partial\phi$. As the \vec{e}_θ and \vec{e}_ϕ components in Eq. (12) are proportional to the second derivatives of V [Eq. (10)], one recognizes that the \vec{m} component of the normal is just zero at $\lambda = \lambda_\pm$. This means that the straight line (9) touches S_+ and S_- tangentially. Moreover, the respective tangential planes to both surfaces are orthogonal. This provides one construction of the solution to the problem (1), once the surfaces S_\pm are drawn. Given the point H representing the field ($\vec{OH} = \vec{h}$), one has to find a straight line going through H and tangent to S_+ and S_- (there will be a discrete number of such lines, as they are the intersection of two cones of apex H). Stability is guaranteed if, starting from H and traveling along the line, one is first tangent to S_+ and then to S_- . The searched magnetization direction \vec{m} is that of this line, oriented from S_+ towards H . This procedure solves the problem (1) in principle. It will be difficult to use with complex surfaces, so that another procedure is described now.

In the Appendix, the surfaces S_+ and S_- are shown to possess another property. They are the focal surfaces (loci of the centers of curvature) of a set of parallel surfaces: the constant energy surfaces in \vec{H} space. This leads to the consideration of a special family of curves on S_\pm , called the focal curves, which correspond to the lines of curvature of the constant energy surfaces. The focal curves cover the surfaces S_\pm , so that each point is crossed by just one of these curves (except for special points). The local tangent to a focal curve is \vec{m} , therefore providing an orientation of the focal curves. This orientation of the tangent allows to solve the \vec{m} problem with one surface only. If one considers S_+ , on which the focal curves are drawn, it suffices in order to solve Eq. (1) to find the point(s) on S_+ where the oriented half tangent to the focal curve crosses H . In Fig. 1 the focal curves have been drawn. These curves in effect split the 3D problem into a collection of nonplanar 2D problems.

B. Energy geometrical calculation

With the aid of the focal curves, the energy of a configuration (\vec{m}, \vec{h}) is easily computed. Indeed, as shown in the Appendix, the energy along a focal curve (on S_+ or on S_-) satisfies

$$dE = -2d\sigma, \quad (13)$$

where E is $V_{\vec{H}}(\vec{m})$ (note that both \vec{h} and \vec{m} vary along a focal curve) and σ is the oriented curvilinear abscissa on the focal curve. Therefore, for a magnetization at an extremum (not only in stable equilibrium) and specializing to S_+ , one can write

$$E = -2(\sigma_+ + \lambda - \lambda_+) + C^{st}, \quad (14)$$

with the notation σ_+ for the curvilinear abscissa on the focal curve drawn on S_+ . The constant is an energy origin, which depends also on the origin of lengths along the focal curve. When many focal curves start from a special point (see Fig. 1 for examples), this point can serve as a common origin of length for these curves. Otherwise, the Appendix shows that a second set of curves is drawn on S_\pm : the constant energy curves. These curves are everywhere orthogonal to the focal curves, and provide a mean to compare energies along different focal curves.

It is now possible to compute the various quantities required in the calculation of the magnetization dynamics. The second order Taylor coefficients of $V_{\vec{H}}$ are easily found first. For a small variation of \vec{m} around an extremum one writes

$$d\vec{m} = d\theta\vec{e}_\theta + \sin\theta d\phi\vec{e}_\phi = du\vec{e}_\theta + dv\vec{e}_\phi. \quad (15)$$

The variation of $V_{\vec{H}}$ is of second order and reads

$$\begin{aligned}dV &= \frac{1}{2}(d\theta)^2 V_{\theta\theta} + d\theta d\phi V_{\theta\phi} + \frac{1}{2}(d\phi)^2 V_{\phi\phi} \\ &= \frac{1}{2}\left[(G_{\theta\theta} + 2\lambda)du^2 + 2\frac{\partial}{\partial\theta}\left(\frac{G_\phi}{\sin\theta}\right)dudv\right. \\ &\quad \left.+ \left(\frac{G_{\phi\phi}}{\sin^2\theta} + \frac{\cos\theta}{\sin\theta}G_\theta + 2\lambda\right)dv^2\right].\end{aligned}\quad (16)$$

A simple calculation, comparing with Sec. II A shows that the symmetric matrix involved has eigenvalues $2(\lambda - \lambda_+)$ and $2(\lambda - \lambda_-)$. The eigenvectors are, as shown in the Appendix, the differential variations of \vec{m} obtained by displacements along the two focal curves on the two focal surfaces. The eigenvalues are the coefficients $c_1^{(i)}$ and $c_2^{(i)}$ of Eqs. (4) and (5). They are as expected positive for a stable equilibrium where $\lambda > \lambda_+ > \lambda_-$. Geometrically, the Taylor coefficients are just (twice) the distance of H to S_+ and S_- , counted on the oriented tangent. Therefore, from a drawing only, the steepness of the local potential well in which \vec{m} sits can be appreciated. As an example the ferromagnetic resonance frequency ω , which corresponds to small oscillations around equilibrium according to the magnetization dynamical equation, is readily found in the case of zero damping to be

$$\begin{aligned}\left(\frac{\omega}{\gamma H_K}\right)^2 &= \frac{V_{\theta\theta}V_{\phi\phi}}{4\sin^2\theta} - \left(\frac{V_{\theta\phi}}{2\sin\theta}\right)^2 = (\lambda - \lambda_+)(\lambda - \lambda_-) \\ &= c_1^{(1)}c_2^{(1)}/4.\end{aligned}\quad (17)$$

This frequency (under the names angular frequency and precession frequency) enters the relaxation time expressions in the thermal¹² and quantum¹⁴ regimes. For the magnetization relaxation theories (thermal or quantum), the Taylor coefficients and barrier height have to be evaluated close to the jump point. A detailed analysis by local geometry, along the lines of Darboux,¹⁷ of the configuration of the critical surface and the focal curves has been used to show that when H comes close to S_+ , only the focal curve ‘‘below’’ H matters (i.e., the curve going through the orthogonal projection of H on S_+). So that it is possible to perform the energy calculations like in 2D.⁵ Figure 2 draws the focal curve and the

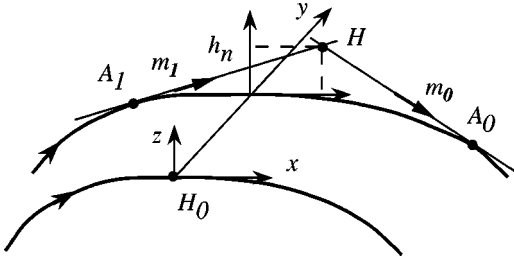


FIG. 2. Local configuration of focal curves and field point close to switching (at H_0). The drawing is in three dimensions. A local surface analysis shows that the focal curve in the same xz plane as H bears the tangents through H (from the points A_1 and A_0), so that the calculation of the curvatures and barriers can be performed in that plane. H is on the stable half tangent through A_1 , but on the saddle-points part of the tangent through A_0 . The focal curves orientation is indicated by arrows.

point H that is moving towards the jump point H_0 . R denotes the radius of curvature of the focal curve at H_0 and h_n the height of point H above the critical surface. To leading order one finds

$$(\lambda - \lambda_+)|_{A_1} = -(\lambda - \lambda_+)|_{A_0} = \sqrt{2Rh_n}. \quad (18)$$

Therefore close to the jump one has $c_2 = -c_2^{(1)}$ and, if S_- is far from H (i.e., $\lambda - \lambda_- \gg |\lambda - \lambda_+|$), $c_1 = c_1^{(1)}$ so that Eq. (4) can be simplified to

$$\tau_0 = 4\pi \frac{\alpha}{\gamma H_K} \frac{1}{c_1^{(1)}} = 2\pi \frac{\alpha}{\gamma H_K} \frac{1}{\sqrt{2Rh_n}}. \quad (19)$$

The other quantity of interest which is the energy barrier is, by the same calculation (the barrier E_B in Sec. I is $Kv\Delta E$, with v the particle volume),

$$\begin{aligned} \Delta E &= V_{\vec{H}}(\vec{m}_0) - V_{\vec{H}}(\vec{m}_1) \\ &= 2(\overline{A_1 H} + \overline{H A_0} - \overline{A_1 A_0}) \\ &= \frac{8\sqrt{2}}{3\sqrt{R}} (h_n)^{3/2} \text{ to leading order.} \end{aligned} \quad (20)$$

The power 3/2 conforms to the general predictions of Victora.¹⁸ The formulas (19) and (20) show that the local magnetization dynamics near a jump point is governed by two factors only: the radius of curvature R of the focal curve on S_+ , at the jump point, and the altitude h_n above that critical surface. In 2D, the curvature radius R could be expressed by a simple formula, but in 3D this becomes too long because of the partial derivatives of λ_+ , so the formula will not be given.

To summarize, the geometrical solution provides:

- the critical surface S_+ at which magnetization jumps occur, explicitly from the expression of the anisotropy, whereas a numerical calculation of the switching field for all orientations would be very demanding;
- two ways to construct the magnetization from the field, graphically;
- the energy of a configuration expressed as a sum of lengths, hence the energy barriers etc.;
- the Taylor coefficients of the potential, as lengths.

III. SPECIAL CASE OF REVOLUTION SYMMETRY

At first sight, the static solution of a revolution problem should be the 2D solution, as by symmetry \vec{m} and \vec{H} have to belong to the same plane. Nevertheless, Stoner and Wohlfarth² in the biaxial case of second degree showed that \vec{m} may rotate out of the plane in certain circumstances. We are now in a position to discuss that point quite generally with the geometrical method.

The revolution axis being chosen as the polar axis for the angles definition, G becomes independent on ϕ . The critical surfaces are described by

$$\lambda_{\pm} = \frac{1}{4} \left[- \left(\frac{\cos \theta}{\sin \theta} G_{\theta} + G_{\theta\theta} \right) \pm \left| \frac{\cos \theta}{\sin \theta} G_{\theta} - G_{\theta\theta} \right| \right]. \quad (21)$$

In the region where $(\cos \theta / \sin \theta) G_{\theta} - G_{\theta\theta} > 0$, the solutions read

$$\lambda_+ = -\frac{1}{2} G_{\theta\theta},$$

$$\vec{h}_+ = \frac{1}{2} G_{\theta} \vec{e}_{\theta} - \frac{1}{2} G_{\theta\theta} \vec{m}, \quad (22)$$

for S_+ , and

$$\lambda_- = -\frac{1}{2} \frac{\cos \theta}{\sin \theta} G_{\theta},$$

$$\vec{h}_- = \frac{1}{2 \sin \theta} G_{\theta} \vec{z}, \quad (23)$$

for S_- . Equation (22) is identical to the general solution of the 2D case.⁵ The surface S_- is here restricted to the axis of S_+ . In the opposite case, S_+ reduces to the axis, which means that the critical surface of a revolution problem may differ from the surface generated by rotation of the 2D critical curve. This result is easily understood. The quantity that has to be positive in order to reproduce the 2D result is, comparing to Eq. (22), $\sin \theta$ (positive as $0 < \theta < \pi$) times the radial component of \vec{h}_+ . If the 2D solution predicts that this component is negative (i.e., of sign opposite to that of \vec{m}), then a π rotation of \vec{m} around the axis will leave G unchanged but increase the dot product $\vec{m} \cdot \vec{h}$, hence reduce the energy. Such a rotation was not allowed in 2D. Figure 3 draws the different critical curves for an anisotropy function $G = \sin^2 \theta \cos^2 \theta$ (it can be obtained as $\sin^2 \theta - \sin^4 \theta$: a strong negative uniaxial anisotropy constant of fourth degree). This case belongs to region VIII of the classification proposed in Ref. 7. In that paper, the hysteresis loops for various values of the two uniaxial anisotropy constants were calculated correctly, but their analysis by a strict 2D formalism gave sometimes different results. The 3D solution when specialized to the revolution symmetry allows for a correct treatment. Figure 4 explains how it is possible to treat revolution symmetry on a 2D drawing. It is helpful to keep on the drawing the part of the 2D critical curve that has been transferred to S_- , in order to define the tangents. There are now two sorts of magnetization jumps, namely the 2D one when the field point crosses the critical curve while meeting the tangency point, and another one (π rotation) if the field point meets

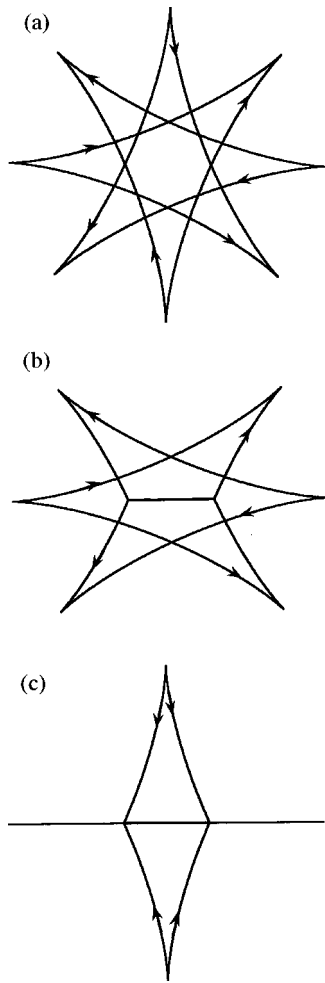


FIG. 3. The three sorts of critical curves in a revolution problem, here with cubic symmetry $G = \sin^2\theta \cos^2\theta$: the usual 2D critical curve (a), the section of the 3D S_+ surface (b) and the section of the 3D S_- surface (c). One sees that some parts of the 2D curve have been transferred to S_- , and that S_+ reduces to the axis in these regions of magnetization angle. The orientation of the 2D curve and of the 3D focal curves is shown by arrows.

the axial section of the critical curve. This new method is more general and precise than the considerations of Ref. 2.

Under revolution symmetry, the focal curves are readily found to be the constant ϕ and constant θ curves, those at constant ϕ corresponding to the 2D critical curve exactly. Therefore these focal curves may travel over S_+ and then over S_- . As this does not affect the energy geometrical calculation, the 3D expression of the barrier height (20) is fully consistent with the 2D result⁵ when the latter applies. The cusp equation (see Sec. A3) for the constant ϕ curves is found immediately to be $(G_{\theta\theta} + G)_{\theta} = 0$, which is also identical to the definition of the cusp points in 2D.⁵

IV. BIAXIAL ANISOTROPY OF SECOND DEGREE

This is the simplest anisotropy that is of 3D nature. Moreover, for nanoparticles made out of materials, like iron or nickel, with a low quality factor (the ratio of anisotropy to magnetostatic energy), a small deviation from a spherical shape leads to a dominant shape anisotropy. The shape anisotropy of a body of arbitrary form is precisely biaxial of

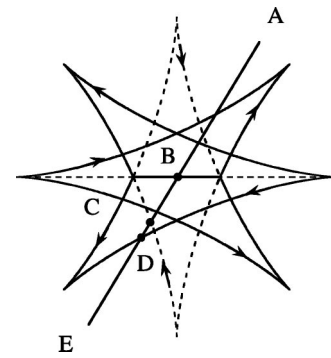


FIG. 4. How to treat a 3D revolution problem with a modified 2D curve, in the same case as Fig. 3. The part of the 2D curve that belongs to S_- has been drawn dashed. The half tangents from that part are stable only after having crossed the revolution axis. A new type of jump (in fact, a π rotation around the axis) occurs when the field point crosses the part of the critical curve that lies on the axis. This jump leaves the component of \vec{M} along \vec{H} unchanged. Jumps are illustrated for a field point moving along a straight line, from A to E. One jump (new type) occurs at B in the revolution case, whereas two jumps (conventional type) are predicted at C and D in the 2D case.

second degree. Thus this case is an important one. The next step will be to know how the addition of small higher degree terms modifies the critical surfaces.

By diagonalization, the anisotropy function can be expressed as

$$G(\vec{m}) = m_x^2 + A m_y^2, \quad \text{with } 0 < A < 1. \quad (24)$$

The easy axis is Oz ; Ox is the hard axis and Oy the intermediate axis. The general shape of S_+ and S_- is shown in Fig. 1(a), as we shall see that these surfaces very much resemble each other whatever A . In particular, S_- is of the same family as S_+ , as it is the S_+ surface of $-G(\vec{m}) = m_z^2 + (1-A)m_y^2$. Straightforward calculations provide the following precise description of S_+ . Cut by the xOy (hard) plane, the surface reduces to a cusp line which is an ellipse of semiaxes having lengths 1 (x direction) and A (y direction). This elliptic cusp line replaces the hard axis cusps of the 2D astroid. The section by the yOz (easy) plane is built out of four focal curves drawing a square astroid of size A . This was expected from the 2D solution. The third section by the xOz plane contains cusp lines and focal curves. The cusp lines are arcs of ellipse, of semiaxes A and $1-A$ in the z and x directions, respectively. They stand in place of the easy axis cusps in the 2D uniaxial case of second degree. The focal curve is an arc of astroid of size 1. Figure 5 superposes these xOz sections for various values of A . The point where the cusp and focal lines meet tangentially is an umbilic. The surface has four umbilics where the ‘‘handle’’ cusps of S_+ and S_- join each other. The focal curves start from the handle cusp and end at the full ellipse cusp, with that orientation. The orientation of the focal curves on S_- is the opposite of that drawn on the rotated S_+ surface with parameter $1-A$.

Considering the $z > 0$ part of S_+ only, one sees that the oriented half tangents cover the whole half space located below the upper part of S_+ , extended by the xOy plane outside the ellipse cusp. Therefore the field points H that are

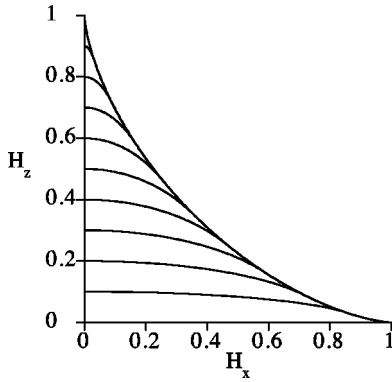


FIG. 5. The sections of a biaxial anisotropy S_+ surface in the plane that contains the easy (z) and hard (x) axes, for values of the parameter A between 0.1 (lower curve) and 0.9. All sections are contained inside an astroid of size 1 and share one part with it. The handle cusp is an arc of ellipse tangent to that astroid. At $A=1$ the problem is of revolution and the 2D astroid is recovered. At $A=0$ (negative uniaxial anisotropy) S_+ reduces to the axis.

located in the exterior of S_+ have exactly one stable solution for \vec{m} , whereas those in the interior have two. The surface S_+ is, as said before, the locus of the field points where a magnetization jump occurs. But, as in 2D, not every crossing of S_+ does give rise to a jump. In this simple case, the rule is easy to derive from the geometrical arrangement of the stable half tangents. Starting from outside S_+ where only one magnetization exists, upon entering inside S_+ the upper or the lower half of the surface will bear the relevant focal curves. Namely, if S_+ is entered from the upper half, the lower part of the surface will carry the focal curves that provide the tangents. Therefore a jump will *only* occur when the field point leaves S_+ through this lower half, for only by this way will a metastable minimum of the potential happen to disappear. This rule is akin to the one often quoted for the 2D square astroid (jump upon exit of the astroid only), although it is more general. At a jump, when H touches the surface, it also meets the focal curve from which the tangent was drawn. The details of the magnetization rotation for any field trajectory can be figured out with little (geometrical) thought. But if exact values are required, numerical calculations are mandatory. The geometrical solution is still of some help however, because instead of a tedious minimization procedure working in all cases one can simply scan in θ and ϕ looking for a half tangent that will touch H (a zero seeking procedure).

If hysteresis cycles are measured for all orientations inside a given plane (like the traditional micro-SQUID (superconducting quantum interference device) measurements^{19,20}), the plot of the measured jump fields within that plane will reproduce a cut of S_+ by the plane. The magnetization just before the jump point is given by the tangent to the focal curve at this point. It does not in general belong to the field plane considered as was the case in 2D. The shape of the curve obtained is also different, it is no longer only composed of arcs of the same concavity joining at cusp points.⁵

In this biaxial case, 2D drawings can be used when the field belongs to the three mirror planes that are left as symmetry elements in Eq. (24). Figure 6 draws these three cuts. The cut of S_- is also shown (dashed), because it helps draw-

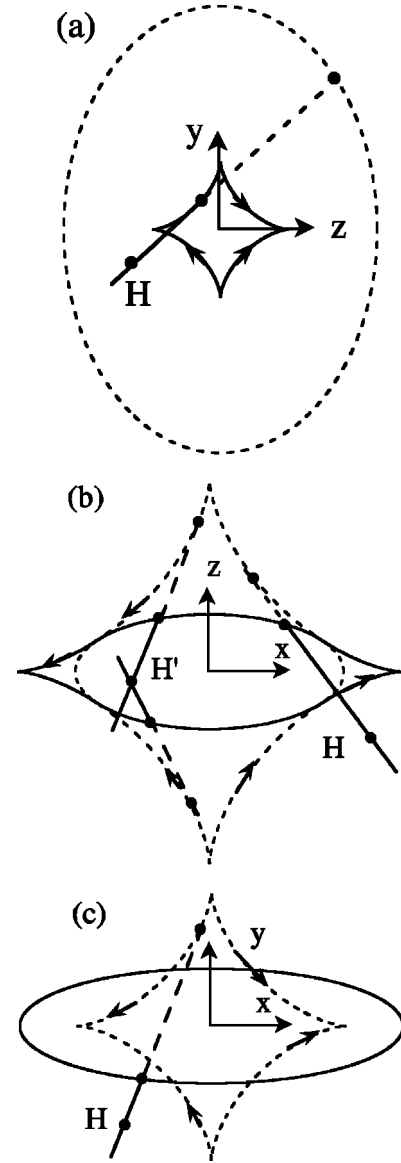


FIG. 6. The three principal cuts of the S_+ (full curves) and S_- (dashed curves) surfaces for a biaxial anisotropy with $A=0.3$ [refer to Fig. 1(a) for a perspective view of the surface]. The construction of the magnetization direction for some field points is shown (the stable half tangent is drawn in full, the part between S_+ and S_- dashed). When the focal curves lie in the cut plane, their orientation is shown (use the mmm symmetry of the surface to have the orientations of all focal curves). The planes are the easy yOz (a), intermediate xOz (b), and the hard xOy planes (c). In (a), the cut of S_- is a cusp, not a focal line, so that the tangent from H to S_- is not tangent to the cut of S_- . The same occurs in (b) and (c) for the S_+ cut.

ing the tangents when the cut of S_+ is a cusp. Notice that in the hard plane cut the magnetization is forced to leave the plane when H is inside S_+ , no stable solution can be constructed otherwise (refer to Sec. II).

V. APPLICATION TO EXPERIMENTAL RESULTS

Although the emphasis of this paper is rather laid on the method itself, it has been felt useful to show some practical

applications of the geometrical objects and tools introduced here.

In the field of nanoparticles, one of the great progress that occurred in the last ten years is the development of techniques allowing particles to be measured individually. Imaging techniques are magnetic force microscopy²¹ and transmission electron microscopy.²² Another one, which is more rapid, consists in measuring the flux from the particle inside a micro-SQUID.²³ This last technique has produced a wealth of hysteresis cycles and switching field angular plots from various nanoparticles or nanowires. As the SQUID can only reproductively work with a small flux, the usual measurement procedure consists in applying fields in the SQUID plane and measuring switching fields versus in plane orientation (see examples in Refs. 19 and 20). As shown by Bonet experimentally,²⁴ field paths more complex than a straight line through the origin are required if all switching fields are desired (cf. also Ref. 5 for the 2D discussion of that point, and Sec. A 3 for a 3D general discussion). A clever indirect procedure was also developed by Bonet.²⁴ When a jump cannot be directly measured (because the flux jump is too small or the necessary field too large for the SQUID to operate), one can see whether the jump has occurred or not by subsequently testing for a jump at a more convenient point that belongs to the same “part” of the focal surface. In Sec. A 3, the 3D discussion of such a procedure is proposed, and the “parts” precisely defined.

Using this indirect technique, 3D switching field surfaces have been measured for the first time on individual nanoparticles.²⁵ The next step is naturally to investigate the magnetization dynamics of these particles, in both thermal and athermal (quantum) regimes. As explained in the Introduction, the determination of the exact anisotropy function is a necessary ingredient for a precise comparison between theories and experiment. For that purpose, the identification of the exact anisotropy from the switching field surface is an attractive possibility. Therefore the two available experimental 3D switching field surfaces (on a Co particle¹⁹ and a BaFeO particle²⁰) have been processed, trying to determine their effective anisotropy function.

A. Recovery of the anisotropy function from the critical surface

In 2D, it has been possible to solve the mathematical problem completely and show how the function $G(\vec{m})$ could be directly found from the critical curve, once the curve is validated as a critical curve (not any astroid-shaped curve is a critical curve⁵). The situation is not as well advanced in 3D, as the answer to the following questions is not known mathematically.

(i) Is S_+ sufficient (without S_- , without the focal curves) to determine G ?

(ii) What are the necessary and sufficient conditions on a surface for being the first critical surface of an anisotropy function?

Let us suppose nevertheless here that the surface has been fully measured, and look for calculated surfaces that resemble it. A first procedure considers the data obtained on one single cut of the 3D surface. For a set of anisotropy parameters and cut orientation, a walk in the (θ, ϕ) rectangle

under the constraint $h_{z'}=0$ (z' denoting the normal to the cut plane, note the cut goes through the origin) calculates a cut. After normalization to the curve length and orientation by some special feature (the maximum radius of the curve for example), the square of the distance between experimental and calculated points at the same curvilinear abscissa is added to build an error. The weight of each experimental point is proportional to its contribution to the curve length. This error is minimized with respect to the parameters by a gradient procedure. It became rapidly clear that one cut is not at all sufficient to determine a whole surface. For example, Fig. 7 shows two fits of equivalent quality of the cut of the surface of the Co particle by the SQUID plane. Both fits were obtained with biaxial second degree and uniaxial fourth degree terms. The corresponding 3D surfaces are extremely different, as are also the determined parameters. Thus a viable procedure has to consider the whole surface. Another disadvantage of the first procedure is that, when some parts are lacking in the experimental curve, the curve length becomes another unknown.

The parameters of the second procedure are those describing the anisotropy function and the three Euler angles accounting for the relative orientations of the experimental and calculated surfaces. The surface size is found as the solution of a 1D least squares problem. Considering the simple shape of the measured surfaces, in case the calculated surface has more than one point in one direction, error is computed with the closest point (note the surface scaling is computed from the unique points only). This time, the weight of the experimental points is taken in proportion of their contribution to the area on the orientation sphere. The surface is calculated as a family of planar cuts that share an axis, as the surface was measured that way and as this allows reusing part of the first procedure. The difficulties of gradient minimization arise from the nonsmoothness of the error as function of the parameters. Both surfaces are indeed known on a finite number of points (about 360 for the experimental, and 2000 for the calculated), and small steps in the error as one integer in the calculation changes by one unit are difficult to avoid completely. The minimization algorithm can become trapped at such artificial minima, and needs often restarting.

The results for the BaFeO particle are presented in Ref. 25. This surface can be described as uniaxial with some deformation. A good reproduction of the surface was obtained with the inclusion of an hexagonal crystalline term of degree 4 plus 6. Here, the results obtained with the Co nanoparticle of Ref. 19 will be described in detail.

B. A cobalt nanoparticle

A first parameters guess can be made from an inspection of the measured surface, with the previous knowledge of the usual critical surfaces. A program computing S_+ for any parameters, whose input was processed by a 3D display software (Silicon Graphics IRIS ExplorerTM), was also of good help. The experimental surface can be described as a revolution astroid that would have been squeezed to nearly half size along the easy axis, that axis being inclined (≈ 20 deg) with respect to the normal to the hard plane nearly circular cusp, and finally the easy axis point being replaced by a short handle cusp. The hard plane cusp was not

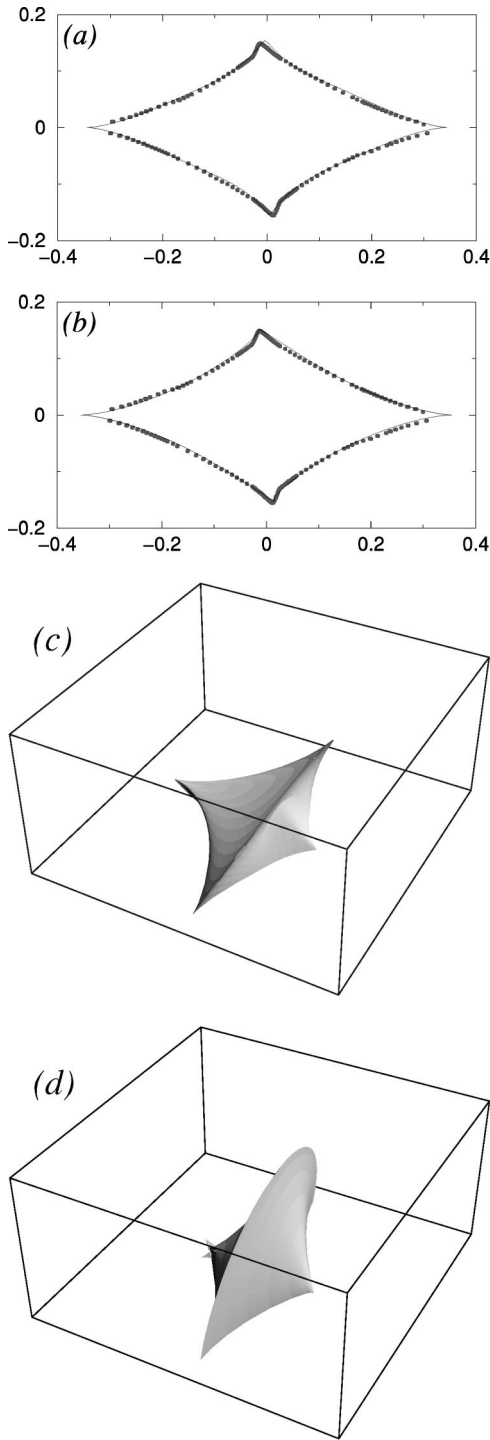


FIG. 7. The distribution of the switching fields for a cobalt nanoparticle (Ref. 19), measured in the micro-SQUID plane, can be fitted alone rather equally well with quite distinct parameters (a) and (b). Points come from experiment and lines from calculation. The corresponding surfaces are shown by their upper half above that plane (c) and (d). The whole experimental surface is closer to (d). The parameters are $A = 0.971$ and 0.645 for the biaxial term and $B = 0.544$ and 1.321 for the uniaxial fourth degree term, respectively. The field scale in (a) and (b) is in Tesla.

measured (see Fig. 7). From Sec. IV, biaxial anisotropy alone cannot reproduce such a surface. If it were of revolution one should have $A = 1$ and the height of the surface should be equal to its diameter. And, if one had $A = 1/2$ to

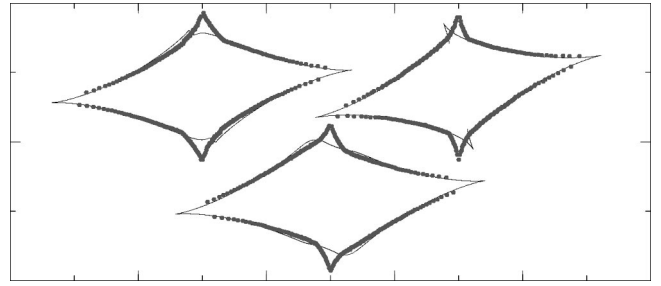


FIG. 8. Results of the fit of the whole switching field surface of the same Co nanoparticle as in Fig. 7. Displayed are three cuts at $\pi/6$ of each other, superposing data (points) and fit (line). The cuts are rotated around the vertical axis of the figure. The fit is obtained with hexagonal symmetry (crystalline terms given by $B \sin^4 \theta + C \sin^6 \theta$).

account for the height and the presence of the easy axis handle cusp, then the hard axis cusp should be an ellipse of aspect ratio 2. Higher-order terms have therefore to be included. Cobalt is hexagonal in bulk form, so that the next order term should be $(m_x^2 + m_y^2)^2$. But recent studies of cobalt nanoparticles^{26,27} indicate that the stable structure in reduced dimensions is cubic (fcc). The next order term should thus be $m_x^2 m_y^2 + m_y^2 m_z^2 + m_z^2 m_x^2$. The anisotropy for cobalt in the fcc phase was determined on thick epitaxial films²⁸ to have a negative constant K_1 , like nickel. The experimental data were fitted with either of these two terms added to a biaxial one. Figure 8 shows 3 representative cuts separated by $\pi/6$ out of the 18 that constitute the surface. This surface fit was performed in the hexagonal crystalline symmetry, with terms of degree 4 and 6 retained. The agreement is quite good, only the easy axis cusp being not fully reproduced (note however that this part is shown in each cut). Under cubic symmetry, a negative magnetocrystalline term was found as expected, but the error was distinctly larger (rms values are 0.02 and 0.04, for a surface half diameter of 1). The fit with the cubic symmetry produces large extra branches close to the easy axis, just like the revolution case when the degree 4 term is strong enough.⁷ This finding of a hexagonal symmetry may be surprising, but it should be reminded that TEM examination of parent cobalt particles showed that not all were of fcc structure,²⁷ and that only one such particle was measured up to now.

This first example, combined with that concerning a barium ferrite nanoparticle,²⁵ shows that a complex anisotropy can indeed be recovered from switching field measurements. However, unambiguous anisotropy identification requires looking carefully for all parts of the surface. One possible such procedure is discussed in the Appendix.

VI. CONCLUSION AND OUTLOOK

We have shown in this paper that a geometrical approach provides a general solution of the coherent magnetization rotation model in 3D. This solution allows for a global understanding of the magnetization behavior (rotation and jump) in field. Moreover, many of the physical quantities of interest have some geometrical signification. For precise values, numerical calculations are of course required. However, we have shown on one example how experimental switching

field surfaces can be fitted by the critical surfaces calculated explicitly from the geometrical technique, in order to extract effective anisotropy parameters that are vital to any modeling of individual nanoparticles.

The mathematical concepts that were used in the course of this work establish a connection with the field of catastrophe theory, singularities and caustics. The caustics analogy is profound. The magnetic constant energy surfaces, being parallel, correspond to the wavefronts of optics. The critical surfaces play thus the same role as caustics. The ‘‘magnetic caustics’’ have the peculiarity of being finite (the optical ones often go to infinity) and of any symmetry.

Finally, all this work was limited to statics, with the exception of the small magnetization vibrations of FMR. How the geometrical method could treat the magnetization dynamics under the classical Landau-Lifshitz-Gilbert equation remains to be investigated.

ACKNOWLEDGMENTS

I would like to thank E. Bonet-Orozco for many inspiring discussions and communication of experimental data, and A. Joets for enlightening discussions on surface geometry. J. Miltat and W. Wernsdorfer should also be thanked for comments and encouragements.

APPENDIX: UNDERLYING MATHEMATICS

1. Constant energy surfaces

It is worthwhile, for many points of view in fact, to consider the surfaces on which $E(\vec{H}) [=V_{\vec{H}}(\vec{m})$ where \vec{m} is an extremum] is constant. The differential of E is $dE = -2\vec{m} \cdot d\vec{h}$ as the variations of \vec{m} disappear because of the extremum condition. Geometrically, this means that the normal to the constant energy surface is \vec{m} . In parametric form, the surface is written as Eq. (9) in which λ is equal to $\lambda(E) = (G-E)/2$. These surfaces are parallel, for if \vec{m} is extremum at a field \vec{h} (energy E), then it is also extremum for fields $\vec{h} + a\vec{m}$ displaced along the surface normal by a length a (energy $E - 2a$).

A well-known surface geometry theorem (see for example Refs. 29, 30, and 17 about surface geometry) states that parallel surfaces have the same loci of curvature centers (the focal surfaces). To find them, we look for the two principal curvatures at each point, through the determination of the lines of curvature (also called principal curves) on the surface. The lines of curvature equation is

$$\frac{d\vec{N}}{ds} = -C_n \vec{t}, \quad (\text{A1})$$

where \vec{N} is the surface normal, s the curvilinear abscissa along the line of curvature, \vec{t} its tangent vector (unitary), and $C_n = 1/\rho$ the normal curvature (ρ the radius of curvature). For the constant energy surfaces, $\vec{N} = \vec{m}$ and expressing \vec{t} through the partial derivatives (12) results in the eigenvalue problem

$$(G_{\theta\theta} + G - E) \frac{d\theta}{ds} + \frac{\partial}{\partial\theta} \left(\frac{G_\phi}{\sin\theta} \right) \sin\theta \frac{d\phi}{ds} = -2\rho \frac{d\theta}{ds},$$

$$\begin{aligned} \frac{\partial}{\partial\theta} \left(\frac{G_\phi}{\sin\theta} \right) \frac{d\theta}{ds} + \left(\frac{G_{\phi\phi}}{\sin^2\theta} + \frac{\cos\theta}{\sin\theta} G_\theta + G - E \right) \sin\theta \frac{d\phi}{ds} \\ = -2\rho \sin\theta \frac{d\phi}{ds}. \end{aligned} \quad (\text{A2})$$

The eigenvalues are, from Eqs. (10) and (11), $\rho_\pm = \lambda_\pm - (G-E)/2 = \lambda_\pm - \lambda(E)$. The associated centers of curvature C_\pm are then simply $\vec{OC}_\pm = \vec{h} + \rho_\pm \vec{N} = \vec{h}_\pm$, where \vec{h}_\pm is given by Eq. (9) with $\lambda = \lambda_\pm$. Thus we find that all the constant energy surfaces have the same focal surfaces (as expected), and that these focal surfaces are just the critical surfaces S_\pm . The matrix of the eigenvalues problem (A2) being symmetric, the two tangent vectors \vec{t}_+ and \vec{t}_- are orthogonal (a general feature of the lines of curvature).

2. Focal surfaces and curves

When the field point H moves on a constant energy surface along a line of curvature, the corresponding center of curvature moves on the corresponding focal surface, along a curve called the focal curve. For each point on S_\pm there exists one and only one focal curve that crosses it. This is because the system (A2) defines the same \vec{t} whatever E , except at special points where the system is degenerate. These points are called umbilics (see for example Refs. 29, 30, and 17): the two surfaces touch at these points, and several or infinitely many focal curves and cusps can meet there. The surfaces S_\pm are therefore covered by the focal curves (‘‘foliated’’ in the vocabulary of Ref. 30). The tangent to the focal curve is found by following its associated line of curvature (hence the notation s_\pm):

$$\frac{d\vec{h}_\pm}{ds_\pm} = \frac{d\vec{h}}{ds_\pm} + \rho_\pm \frac{d\vec{m}}{ds_\pm} + \frac{d\rho_\pm}{ds_\pm} \vec{m} = \frac{d\rho_\pm}{ds_\pm} \vec{m} \quad (\text{A3})$$

[the last equality results from the line of curvature definition (A1)]. The tangent is thus directed along \vec{m} and we can choose this direction to orient the focal curve.

To obtain the tangent plane to the focal surface, \vec{h}_\pm is derived with respect to a displacement along the other line of curvature, resulting in

$$\frac{d\vec{h}_\pm}{ds_\mp} = (1 - \rho_\pm/\rho_\mp) \vec{t}_\mp + \frac{d\rho_\pm}{ds_\mp} \vec{m}. \quad (\text{A4})$$

The tangent vector to the line of curvature is thus the normal to its associated focal surface. As \vec{t}_+ and \vec{t}_- are orthogonal, so are the tangent planes to S_+ and S_- .

Is the focal curve a special curve on the focal surface? The equation of the lines of curvature, interpreted on S_\pm where \vec{m} is the tangent vector to the focal curve and \vec{t}_\pm the surface normal, means that the focal curve is a geodesic curve of its focal surface (see, e.g., Refs. 29, 30, and 17 for the definition). This does not characterize the focal curves fully, however, as a geodesic curve can be constructed with any tangent through a surface point.

Let us denote by σ_\pm the oriented curvilinear abscissa on the focal curves. By definition, one has from Eq. (A3)

$$\frac{d\sigma_{\pm}}{ds_{\pm}} = \frac{d\rho_{\pm}}{ds_{\pm}}. \quad (\text{A5})$$

As the energy on a point on the focal surface is related to that of the constant energy surface by $E(C_{\pm}) = E - 2\rho_{\pm}$, the energy variation along the focal curves is directly that of the oriented curvilinear abscissa

$$dE = -2d\sigma_{\pm}. \quad (\text{A6})$$

This last relation (A6) forms the basis of the energy geometrical calculation in three dimensions.

The orthogonal trajectories of the focal curves, on their focal surface, are also of interest. On S_{\pm} , \vec{t}_{\pm} is the surface normal, \vec{m} the tangent to the focal plane and therefore the tangent to the orthogonal curve is \vec{t}_{\mp} . So that, from Sec. A 1, the energy variation along this normal trajectory is zero and the orthogonal trajectories of the focal curves are constant energy curves. Note finally that, from Eq. (A4), these orthogonal trajectories are not obtained by a mere displacement of the point on the constant energy surface along the other line of curvature.

3. Cusps on the focal surfaces

The oriented curvilinear abscissa changes orientation at the points satisfying

$$\frac{d\rho_{\pm}}{ds_{\pm}} = \frac{d\theta}{ds_{\pm}} \frac{\partial}{\partial\theta}(\lambda_{\pm} - G/2) + \frac{d\phi}{ds_{\pm}} \frac{\partial}{\partial\phi}(\lambda_{\pm} - G/2) = 0, \quad (\text{A7})$$

where the derivatives with respect to s_{\pm} are provided by the solutions of Eq. (A2). This assumes that nothing occurs on the line of curvature, i.e., that the point considered is not an umbilic. Eq. (A7) defines cusp lines through a relation between θ and ϕ . These lines are very visible on the drawings of the focal surfaces (see Fig. 1) where they generalize the cusp points of the 2D critical curve. They are called ‘‘ribs’’ in Ref. 30. But on the constant energy surfaces their ‘‘ridges,’’³⁰ counterparts are not apparent.

The drawings of Fig. 1 make it clear that the critical surfaces S_{\pm} can be thought of as made of parts that are glued tangentially along certain cusps. Each part consists of one cusp (or three cusps³⁰) from which focal lines start, and one or several cusps on which they end. From their shape in the biaxial case, one may call these parts of focal surface ‘‘bells’’ (the cubic case where the handle cusp reduces to a point is a very high symmetry one). The stable half tangents out of one bell reach once every point of a domain which is the inside of the bell extended by the half tangents emanating from the end cusp(s). As long as a field point stays inside the domain of a given bell, the jumps of magnetization shall occur only when that point crosses the bell surface. Each bell corresponds to a family of magnetizations, where one can go continuously from one to another direction. A bell thus

means one phase of the magnetic phase theory,¹⁶ i.e., roughly one magnetization state (but not necessarily obtained in zero field). Thinking of the critical surface in terms of bells has the advantage of simplifying the geometrical reasoning greatly. The two bells of the biaxial surface were already considered in Sec. IV. The cubic S_{+} surface likewise consists of six fourfold symmetrical bells where the starting cusp is an umbilic of high symmetry (there are additionally eight small threefold symmetrical bells on the $\{111\}$ orientations).

The decomposition of the surface into bells also allows to understand how the whole surface could be measured, even with a SQUID and despite the very small magnetization jumps at the hard axis cusps. For each bell, one needs to have one point of its surface that gives rise to a measurable jump (call it the test point). For the micro-SQUID technique, the test point has to belong to the SQUID plane. Additionally, one point inside the bell (called center point), reached by coming from the bell domain at infinity, has to be found in order to reset the magnetization after a jump. One possible measurement procedure is to increase field from the center point in all directions up to the bell. Whether one has reached the bell or not can be tested by going back to the center and testing for a jump at the test point (provided the journey back to the test point is contained inside the domain of the new bell after the jump). This justifies the indirect measurement procedure of Ref. 24. For the bells that do not cross the SQUID plane, or with non measurable jumps in this plane, or which intersect, more indirect procedures have to be designed. It appears thus that the knowledge of what critical surfaces should look like is necessary to guide the experimentalist in devising the measurement procedure, like in Ref. 24.

We have been naturally led to a separation of the cusp lines into two sorts, namely those from which the focal lines depart and those where they end. In the 2D case,²⁴ Bonet called the second sort the ‘‘choice’’ lines, for whether the critical surface is entered from above or below such lines one will get different magnetizations at the same point. It is clear from the above discussion that a general description and classification of the cusp lines in relation with our problem would be very useful (the classification by Porteous³⁰ could well be just that). But this is beyond the scope of this paper.

More generally, one should note that the arrangement of the cusp lines is one topic of catastrophe theory. The no symmetry case (called generic by the mathematicians) has been studied long ago. Recently also,³¹ symmetrical cases have been investigated. This related work is not a mere mathematical curiosity, for it provides general rules concerning the architecture of the cusp lines, which are the backbone of the focal surfaces and play a key role in the magnetization rotation processes as just seen. For example, the ways in which a cusp line may transform under changes of G are mathematically fixed by Catastrophe theory.

¹W. Brown, Jr. and A. Morrish, Phys. Rev. **105**, 1198 (1957).

²E. Stoner and E. Wohlfarth, Philos. Trans. R. Soc. London, Ser. A **240**, 599 (1948).

³D. Smith, J. Appl. Phys. **29**, 264 (1958).

⁴C. Johnson and W. Brown, Jr., J. Appl. Phys. **32**, 2435 (1961).

⁵A. Thiaville, J. Magn. Magn. Mater. **182**, 5 (1998).

⁶J. Slonczewski (unpublished).

⁷C. Chang, J. Appl. Phys. **69**, 2431 (1991).

⁸R. Kodama, A. Berkowitz, E. McNiff, Jr., and S. Foner, Phys. Rev. Lett. **77**, 394 (1996).

- ⁹L. Del Bianco *et al.*, J. Appl. Phys. **84**, 2189 (1998).
- ¹⁰R. Kodama, S. Makhlof, and A. Berkowitz, Phys. Rev. Lett. **79**, 1393 (1997).
- ¹¹L. Geoghegan, W. Coffey, and B. Mulligan, Adv. Chem. Phys. **100**, 475 (1997).
- ¹²W. Coffey, Adv. Chem. Phys. **103**, 259 (1998).
- ¹³W. Coffey *et al.*, Phys. Rev. Lett. **80**, 5655 (1998).
- ¹⁴G. Kim and D. Hwang, Phys. Rev. B **55**, 8918 (1997).
- ¹⁵G. Kim, J. Appl. Phys. **84**, 391 (1998).
- ¹⁶A. Hubert and R. Schäfer, *Magnetic Domains* (Springer, Berlin, 1998), Secs. 3.4.3–4.
- ¹⁷G. Darboux, *Théorie Générale des Surfaces* (in french) (reprinted by Chelsea, New York, 1972), Vol. V, Chap. II.
- ¹⁸R. Victora, Phys. Rev. Lett. **63**, 457 (1989).
- ¹⁹W. Wernsdorfer *et al.*, Phys. Rev. Lett. **78**, 1791 (1997).
- ²⁰W. Wernsdorfer *et al.*, Phys. Rev. Lett. **79**, 4014 (1997).
- ²¹M. Lederman, G. Gibson, and S. Schultz, J. Appl. Phys. **73**, 6961 (1993).
- ²²S. Majetich and Y. Jin, Science **284**, 470 (1999).
- ²³W. Wernsdorfer *et al.*, J. Magn. Magn. Mater. **145**, 33 (1995).
- ²⁴E. Bonet Orozco *et al.*, IEEE Trans. Magn. **34**, 979 (1998).
- ²⁵E. Bonet, W. Wernsdorfer, B. Barbara, A. Benoît, D. Mailly, and A. Thiaville, Phys. Rev. Lett. **83**, 4188 (1999).
- ²⁶O. Kitakami *et al.*, Jpn. J. Appl. Phys., Part 1, **35**, 1724 (1996).
- ²⁷N. Demoncey *et al.*, Eur. Phys. J. B **4**, 147 (1998).
- ²⁸T. Suzuki *et al.*, Appl. Phys. Lett. **64**, 2736 (1994).
- ²⁹J. Stoker, *Differential Geometry, Pure and Applied Mathematics* (Wiley Interscience, New York, 1969), Vol. XX.
- ³⁰I. Porteous, *Geometric Differentiation* (Cambridge University Press, Cambridge, 1994).
- ³¹A. Joets, M. Monastyrsky, and R. Ribotta, Phys. Rev. Lett. **81**, 1547 (1998).